

Supporting Information For

Thermodynamic Origin of Irreversible Magnesium Trapping in Chevrel Phase Mo_6S_8 : Importance of Magnesium/vacancy Ordering

Chen Ling ^{1,*} and Koji Suto ¹

¹ Toyota Research Institute of North America, 1555 Woodridge Ave, Ann Arbor, Michigan, United States,
48105

Corresponding Author: chen.ling@toyota.com

S.1 Rate performance of Mo₆S₈ cathode in high voltage and low voltage regime

In order to show the rate performance of CP Mo₆S₈ cathode, we re-plotted the data from Figure 3b in Ref. S1 (ref. 27 in the main manuscript), which reported the capacity of nanosized CP as a function of cycling rate (C rate). As shown in Figure S1, it is apparent that the CP cathode exhibited better rate capability in low voltage regime in terms of both capacity retention, defined as the capacity normalized by that at 0.1 C rate and capacity decay, defined as the decreased capacity compared to that at 0.1 C rate.

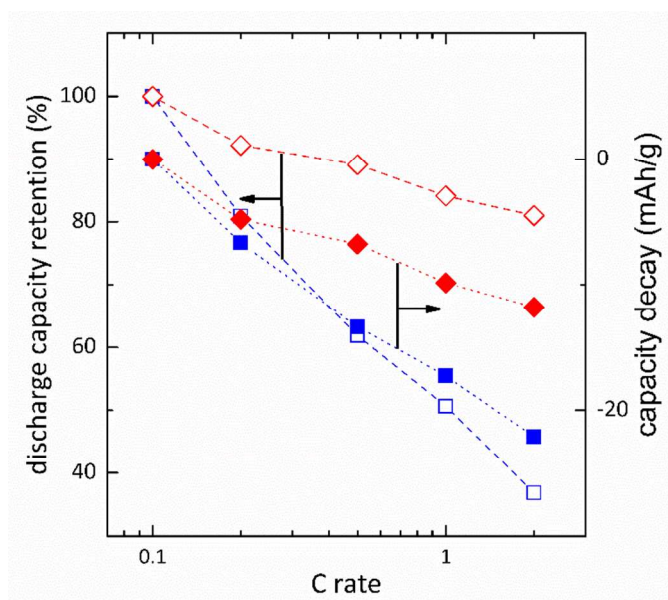


Figure S1. Rate performance of CP Mo₆S₈ cathode in high voltage (blue) and low voltage (red) regimes. Data is re-plotted from reference S1.

S.2 AIMD trajectory of Mg at different compositions

Figure S2 shows the trajectory of Mg atoms in AIMD simulation at two different compositions. At low Mg concentration only a few hopping events were observed. The trajectory did not percolate the lattice. In sharp contrast, at high concentration a percolating trajectory was observed.

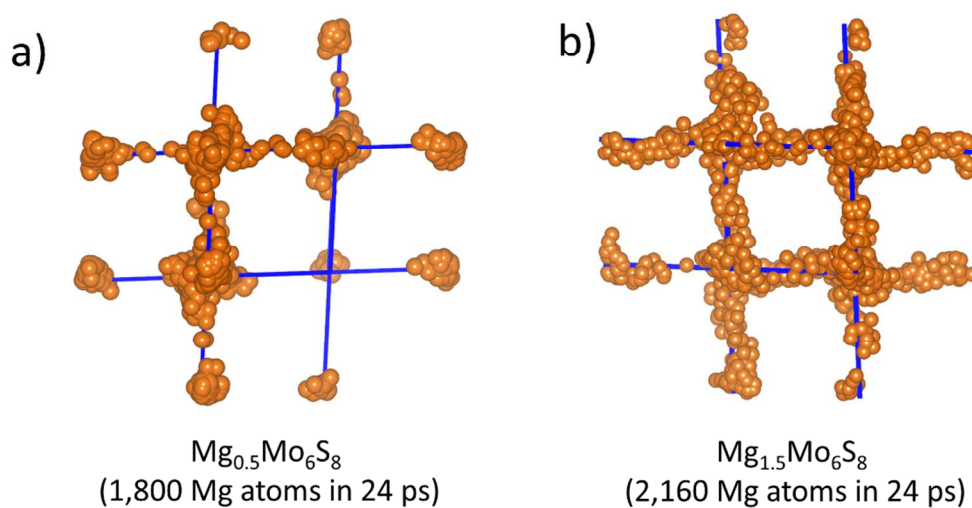


Figure S2. Trajectory of Mg in AIMD simulations. The blue lines show the 3a sublattice in CP structure. For simplicity Mo and S atoms are omitted. The snapshots were taken every 160 fs or 40 MD steps for (a) and 400 fs or 100 MD steps for (b).

S.3 Site preference in high voltage regime

The CP structure contains several interstitial sites for the insertion of Mg. To examine the site preference, we calculated the energy difference at the composition of $\text{Mg}_{0.33}\text{Mo}_6\text{S}_8$ and $\text{Mg}_1\text{Mo}_6\text{S}_8$. For $\text{Mg}_{0.33}\text{Mo}_6\text{S}_8$, one Mg was initiated at inner site, outer site, 3a and 9d positions in the supercell of $\text{Mg}_1\text{Mo}_{18}\text{S}_{24}$. For $\text{Mg}_1\text{Mo}_6\text{S}_8$, three Mg was initiated at inner site, 3a and 9d positions in the supercell of $\text{Mg}_3\text{Mo}_{18}\text{S}_{24}$. Because of the large number of possible configurations the occupancy of outer site at $\text{Mg}_1\text{Mo}_6\text{S}_8$ was not analyzed. Table S1 reported the relative energy for different interstitial sites. For both compositions we found that the inner site is the most stable, in good agreement with previous experimental studies.^{S2}

Table S1. Relative energy of $\text{Mg}_x\text{Mo}_6\text{S}_8$ (unit: eV) at $x=0.33$ and $x=1$.

	inner site	outer site	3a	9d
$\text{Mg}_{0.33}\text{Mo}_6\text{S}_8$	0	0.095	0.670	0.545
$\text{Mg}_1\text{Mo}_6\text{S}_8$	0	-	0.887	1.033

S.4 Vibrational frequencies of Mg at 9d site

To examine whether 9d site is a saddle point or a local minimum at low Mg concentrations, we calculated the vibrational frequency of Mg atoms. In our calculation, one Mg atom was initiated at 9d site and the geometry was optimized by allowing all atoms to relax. Due to symmetric confinement that Mg atom stayed at 9d after relaxation. Afterwards, the positions for all other atoms were fixed and a small displacement was added to that Mg atom. The vibrational frequency was calculated under harmonic approximation. Table S2 shows the frequency for two compositions. In both cases we found an imaginary frequency and two real frequencies, demonstrating 9d is indeed a saddle point. For comparison, Table S2 also shows the frequencies for Mg at inner site, where all frequencies are real.

The calculated frequencies allow us to estimate the hopping rate as

$$\Gamma = \frac{\prod_{i=1}^{i=3} f_i}{\prod_{j=1}^{j=2} f_j} \exp(-\beta E_a)$$

where f_i and f_j is the real vibrational frequency at inner site and transition state, respectively. With Equation S1 the pre-exponential part was calculated to be $2.2 \times 10^{12} \text{ s}^{-1}$ and $2.6 \times 10^{12} \text{ s}^{-1}$ at the composition of $\text{Mg}_{0.0833}\text{Mo}_6\text{S}_8$ and $\text{Mg}_{0.9167}\text{Mo}_6\text{S}_8$, respectively. We used the average value of $2.4 \times 10^{12} \text{ s}^{-1}$ to estimate the diffusivity using Equation 8 in the main manuscript.

Table S2. Vibrational frequencies (unit: $\times 10^{12}$ Hertz) of Mg in CP. The unit i indicates imaginary frequency.

		f_1	f_2	f_3
9d	$\text{Mg}_{0.0833}\text{Mo}_6\text{S}_8$	13.58	4.92	1.34i
	$\text{Mg}_{0.9167}\text{Mo}_6\text{S}_8$	12.27	5.09	1.13i
Inner site	$\text{Mg}_{0.0833}\text{Mo}_6\text{S}_8$	7.71	5.94	3.20
	$\text{Mg}_{0.9167}\text{Mo}_6\text{S}_8$	8.84	6.17	3.01

S.6 Convex hull of Mg insertion from $\text{Mg}_0\text{Mo}_6\text{S}_8$ to $\text{Mg}_1\text{Mo}_6\text{S}_8$

We applied the convex hull method to generate the ground states for Mg insertion from $\text{Mg}_0\text{Mo}_6\text{S}_8$ to $\text{Mg}_1\text{Mo}_6\text{S}_8$. In the convex hull method, the energies for a group of distinct configurations were calculated and the convex hull was created by creating the relative energy profile as a function of Mg concentration. The relative energy was obtained using

$$E = E_x - (1 - x)E_0 - xE_1 \quad (\text{S2})$$

where E_x , E_0 and E_1 is the DFT energy for $\text{Mg}_x\text{Mo}_6\text{S}_8$, $\text{Mg}_0\text{Mo}_6\text{S}_8$ and $\text{Mg}_1\text{Mo}_6\text{S}_8$, respectively. For $\text{Mg}_1\text{Mo}_6\text{S}_8$ we used the lowest energy from Figure S3 as the reference state in calculation.

Figure S4 shows the ground states identified in current work. A total of 92 configurations were calculated. Besides $\text{Mg}_0\text{Mo}_6\text{S}_8$ and $\text{Mg}_1\text{Mo}_6\text{S}_8$, three more ground states are found at $x=0.33$, 0.5 and 0.67. Analyzing the filling of 3a lattice at the ground states and during AIMD simulation gives the intercalation pathway as shown in Figure 5b in the main manuscript.

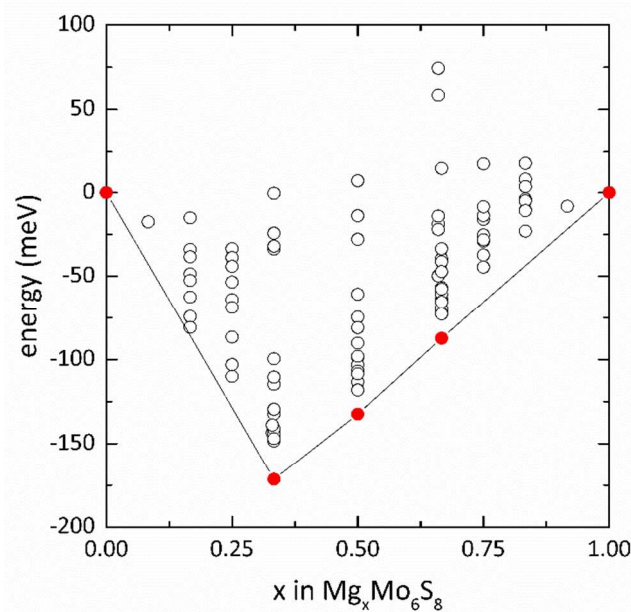


Figure S4. Convex hull of Mg insertion from $\text{Mg}_0\text{Mo}_6\text{S}_8$ to $\text{Mg}_1\text{Mo}_6\text{S}_8$.

Figure S5 shows the predicted voltage profile considering the intermediates states between $x=0$ and $x=1$. The voltages were calculated with only the formation energies without considering the entropy contribution. We observe a drop of 0.17 V at $x=0.333$. From $x=0.333$ to $x=1$, the predicted voltage showed small variation of 0.04 V. The experimental voltage profile from reference S1 showed a plateau from $x=0$ to $\sim x=0.5$ and then dropped to the low voltage regime. Considering typical DFT error for the voltage prediction is around 0.1-0.2 V, we consider our prediction at least qualitatively agreed with the experiments. A detailed experimental study will provide more conclusive evidence about the phase behavior at room temperatures as being discussed in the manuscript.

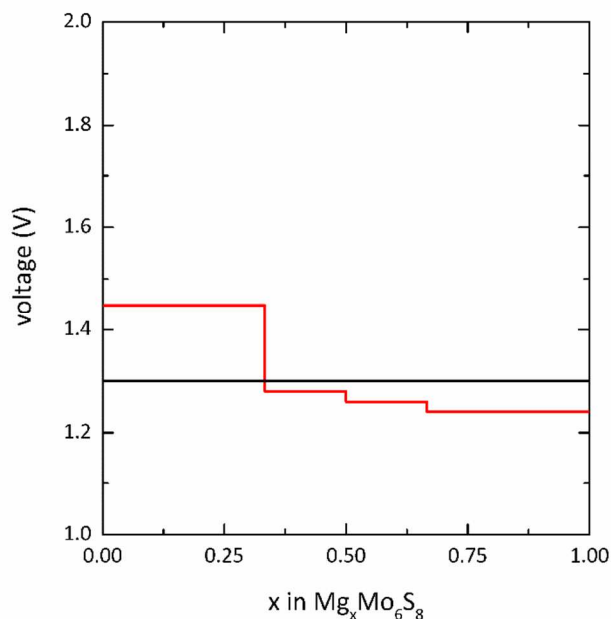


Figure S5. Predicted voltage profile (red) and average voltage (black) from $Mg_0Mo_6S_8$ to $Mg_1Mo_6S_8$.

Reference:

(S1). Cheng, Y.; Parent, L. R.; Shao, Y.; Wang, C.; Sprenkle, V. L.; Li, G.; Liu, J. Facile Synthesis of Chevrel Phase Nanocubes and Their Applications for Multivalent Energy Storage.

Chem. Mater. **2014**, *26*, 4904-4907

(S2). Levi, E.; Lancry, E.; Mitelman, A.; Aurbach, D.; Ceder, G.; Morgan, D.; Isnard, O. Phase Diagram of Mg Insertion into Chevrel Phases, $Mg_xMo_6T_8$ (T =S, Se). 1. Crystal Structure

of the Sulfides. *Chem. Mater.* **2006**, *18*, 5492-5503